J. Mol. Biol. (1995) **248**, 887–900

JMB

Towards the Molecular Architecture of the Asymmetric Unit Membrane of the Mammalian Urinary Bladder Epithelium: A Closed ''Twisted Ribbon'' Structure

Thomas Walz[1], Markus Häner[1], Xue-Ru Wu[2], Christian Henn[1] Andreas Engel[1], Tung-Tien Sun[3] and Ueli Aebi[1,4]*

[1]*M. E. Müller Institute for Structural Biology Biozentrum, University of Basel, CH-4056 Basel Switzerland*

[2]*Departments of Urology and Microbiology, New York University School of Medicine, New York NY 10016, USA.*

[3]*Epithelial Biology Unit Departments of Dermatology and Pharmacology, Kaplan Cancer Center, New York University School of Medicine, NY 10016, USA*

[4]*Department of Cell Biology and Anatomy, Johns Hopkins University School of Medicine, Baltimore MD 21205, USA*

**Corresponding author*

The asymmetric unit membrane (AUM) forms numerous plaques covering the apical surface of mammalian urinary bladder epithelium. These plaques contain four major integral membrane proteins called uroplakins Ia, Ib, II and III, which form particles arranged in a well-ordered hexagonal lattice with p6 symmetry and a lattice constant of 16.5 nm. Bovine AUM plaques negatively stained with anionic sodium silicotungstate revealed structural detail to 3.1 nm resolution. Correlation averaging resolved each particle into 12 stain-excluding domains arranged in two concentric rings (inner ring radius (r_{in})=3.7 nm, outer ring radius (r_{out}) = 6.6 nm), each with six domains which were rotated by roughly 30° relative to each other. Negative staining with cationic uranyl formate increased the resolution to 2.2 nm and unveiled distinct connections between adjacent AUM particles. These connections may provide a molecular basis for the observed insolubility of the plaques in many detergents. Examination of the luminal face of freeze-dried / unidirectionally metal-shadowed AUM plaques established a left-handed vorticity of the 16 nm protein particles, whereas the cytoplasmic face exhibited no significant surface corrugations. Three-dimensional reconstruction from sodium silicotungstate-stained specimens revealed the AUM particles to be built of six ''V-shaped''subunits anchored upright in the membrane. The mass density distribution within uranyl formate-stained AUM particles was similar except that the inner tip of each V was bridged to the outer tip of an adjacent V, so that the 16 nm AUM particle appeared as a continuous, ''twisted ribbon'' embracing a central cavity. Finally, mass measurements of unstained / freeze-dried plaques by scanning transmission electron microscopy yielded a total mass of 1,120 kDa per membrane-bound AUM particle. By imposing constraints on the possible uroplakin stoichiometries within AUM plaques, these data provide a first glimpse of the molecular architecture of the 16 nm particles constituting the plaques.

Keywords: asymmetric unit membrane; electron microscopy; 3D image reconstruction; 2D membrane crystals; uroplakins

Introduction

Integral membrane proteins perform many important biological functions. For example, they maintain the electrochemical gradient, mediate the transport of nutrients, transduce signals, establish cell–cell interactions, and link the membrane to the cytoskeleton. Such a variety of functions requires membrane proteins of diverse structures. Whereas the functions are well known in many cases, the atomic structure of only a few membrane proteins has been determined to date. On the one hand, X-ray crystallography has solved the atomic structure of the bacterial photosynthetic reaction center (Deisenhofer *et al*., 1984, 1985), and of several bacterial porins (Weiss *et al*., 1991; Cowan *et al*., 1992), but the problems associated with growing large,

Abbreviations used: AUM, asymmetric unit membrane; UP, uroplakin; PTA, phosphotungstic acid; UF, uranyl formate; EM, electron microscopy; STEM, scanning transmission electron microscopy; SST, sodium silicotungstate; MPA, mass per area; MPU, mass per unit cell; RCF, radical correlation function; 2D, 3D, two- and three-dimensional.

0022–2836 / 95 / 200877–14 $08.00 / 0

well-ordered, three-dimensional (3D) crystals of integral membrane proteins have thus far prevented rapid progress. On the other hand, electron crystallography has produced an atomic structure of bacteriorhodopsin (Henderson *et al*., 1990), and of a light harvesting complex (Kühlbrandt *et al*., 1994). Hence, electron crystallography has evolved into a viable alternative for determining the atomic structure of integral membrane proteins, particularly since strategies for growing two-dimensional (2D) crystals of membrane proteins in the presence of phospholipids have been improved significantly over the past few years (Jap *et al*., 1992; Kühlbrandt, 1992; Engel *et al*., 1992).

A mammalian biomembrane particularly amenable to detailed structural analysis is the specialized plaque of the urinary bladder epithelium (also known as the urothelium). A large portion of the luminal plasma membrane of this urothelium is covered with scallop-shaped plaques (Vergara *et al*., 1969; Hicks & Ketterer, 1969; Staehelin *et al*., 1972; Knutton & Robertson, 1976) which are typically 0.3 to 0.5 μm in diameter (Hicks, 1965). These rigid-looking plaques are interspersed by flexible plasma membrane segments, called ''hinge'' areas (Porter & Bonneville, 1963). When viewed in transverse section, plaque membranes appear much thicker than the membranes of the hinge area, because the luminal leaflet of the plaques is approximately twice as thick as the cytoplasmic one, hence the name ''asymmetric unit membrane'' (AUM) arose (Hicks, 1965). Freeze-etching (Staehelin *et al*., 1972; Robertson & Vergara, 1980) and negative staining (Vergara *et al*., 1969; Hicks & Ketterer, 1969) of isolated luminal plaques have demonstrated that they are composed of distinct protein particles, approximately 12 nm in diameter†, which form a well ordered hexagonal lattice (Caruthers & Bonneville, 1980). Thus, the AUM represents one of the few examples of a mammalian membrane whose protein subunits naturally form a 2D crystal *in situ*. Another useful feature of the AUM is that, as a biomembrane, it has a relatively simple protein composition. We have shown recently that bovine AUM contains four major protein subunits; the 27 kDa uroplakin (UP) Ia, the 28 kDa UPIb, the 15 kDa UPII and the 47 kDa UPIII (Yu *et al*., 1990; Yu *et al*., 1994; Wu *et al*., 1990). Molecular cloning and sequencing data have established that UPIa and UPIb, which share 39% of their amino acid sequence, belong to a superfamily of integral membrane proteins all possessing four transmembrane segments (Yu *et al*., 1994). In contrast, the 15 kDa UPII contains only one potential transmembrane segment located at its C terminus (Lin *et al*., 1994). The only potential transmembrane segment of the 47 kDa UPIII is also located near its C terminus (Wu & Sun, 1993). The transmembrane topology of the uroplakins was investigated by electron microscope (EM) localization and by exploring the protease accessibility of UPs that were inserted *in vitro* co-translationally into dog pancreatic vesicles (Lin *et al*., 1994; Yu *et al*., 1994). The emerging data suggest that all major hydrophilic domains of UPIa, UPIb and UPII are exposed to the luminal space with practically no cytoplasmic tail. Most of the hydrophilic domain (i.e. consisting of the 189-residue, N-terminal part) of UPIII is also exposed luminally. The extracellular domains of the UPs probably interact with one another to form the 16 nm AUM particles (Wu & Sun, 1993; Yu *et al*., 1994). Since UPIII is the only uroplakin that possesses a significant, 50-residue cytoplasmic tail, this domain may mediate the interaction of the AUM with the cytoskeleton (Wu & Sun, 1993). Finally, since AUM is the major differentiation product of mammalian urothelium, and since it remains insoluble in many detergents that can dissolve other biomembranes, large amounts of highly purified and morphologically intact AUM can be isolated routinely (~10 mg in a day; Wu *et al*., 1990; Wu *et al*., 1994).

Therefore, AUM provides an excellent model system for investigating how several mammalian integral membrane proteins, in this case the four uroplakins, interact with one another and assemble into a highly organized supramolecular structure. By studying the *in vivo* 2D crystalline structure of AUM using digital image processing, it was established that each stellate-shaped particle can be resolved into six inner and six outer domains, and that these particles form a crystalline arrangement with p6 symmetry and a 16.5 nm center-to-center spacing (Vergara *et al*., 1969; Hicks & Ketterer, 1969). Using electron micrographs collected from tilted AUM plaques that had been negatively stained with phosphotungstic acid (PTA), Brisson & Wade (1983) and Taylor & Robertson (1984) reconstructed 3D models of the 16 nm AUM particle. Specifically, they showed that each of the 6-fold symmetrical 16 nm protein particles consists of 12 domains, with six being arranged in an inner ring (inner ring radius (r_{in}) = 3.5 nm) and six in an outer ring (outer ring radius (r_{out}) = 6 nm), and that each inner domain is connected to a corresponding outer domain. However, the resolution of these 3D reconstructions was too low (~3 nm) to discern the detailed spatial organization of the inner and outer domains.

In this paper, we show that the resolution of 2D projection maps of AUM plaques can be improved by using uranyl formate (UF), instead of PTA, as the negative stain. Corresponding correlation-averaged projection maps revealed the 16 nm particles to be interconnected. This distinct inter-particle interaction may contribute significantly to the remarkable insolubility of AUM plaques in many detergents. The 3D mass density map of the 16 nm particle computed from images of UF-stained AUM plaques revealed a closed ''twisted ribbon'' embracing a central cavity. Metal-shadowing data mainly high-

† Although these luminal particles have been described as having a diameter of 12 nm, unit cell measurements revealed a lattice constant or center-to-center distance of ~16 nm. We will therefore hitherto call these particles 16 nm particles.

lighted the six elevations of the twisted ribbon that correspond to the six inner domains of the 16 nm particle, thus providing strong support for the model deduced from the 3D reconstructions. Finally, we measured the mass of the membrane-bound 16 nm AUM particles by quantitative scanning transmission electron microscopy (STEM) yielding a value of 1120 kDa per unit cell. The structural implications of these results on the molecular architecture of the 16 nm particles constituting the AUM plaques will be discussed.

Results

Two-dimensional projections of bovine AUM plaques

In an effort to improve the resolution of the structural detail, we negatively stained bovine AUM plaques not only with sodium silicotungstate (SST) (Figure 1a to c), a traditional anionic heavy metal salt, but also with UF (Figure 1d to i), a typical cationic heavy metal salt. Although both stains revealed the same hexagonal lattice with unit cell dimensions of $a = b = 16.5$ nm, the relative intensities of corresponding reciprocal lattice reflections of computed diffraction patterns were distinct (Figure 1b, e and h).

Accordingly, the best SST-stained plaques diffracted to the 4,1 reciprocal hexagonal lattice order (Figure 1b) corresponding to a resolution of 3.1 nm. Correlation-averaged unit cells computed from such SST-stained plaques (Figure 1c) exhibited strong 6-fold symmetry, i.e. the deviation from 6-fold symmetry was usually less than 1%. Each unit cell contained two distinct sets of six stain-excluding domains: the six inner, more massive domains joined to form an inner ring with their centers of mass at a radius $r_{in} = 3.7$ nm, whereas the six outer, more tenuous domains were arranged on an outer ring with their centers of mass at a radium $r_{out} = 6.6$ nm. The two rings were rotated by roughly 30° relative to their corresponding centers of mass. The inner and outer stain-excluding domains were both roughly circular in shape, and had an average diameter of 3.3 nm and 2.7 nm, respectively. The six inner domains joined each other via a distinct stain-excluding bridge at a radius of 3.1 nm, and their centers of mass were skewed by about 10° clockwise relative to the hexagonal lattice lines. Similarly, the six outer domains were skewed by approximately 20° anti-clockwise relative to the hexagonal lattice lines. These results confirmed and extended those of Brisson & Wade (1983) and Taylor & Robertson (1984), who used the anionic heavy metal salt phosphotungstic acid as a negative stain.

In contrast, the best UF-stained plaques diffracted to the 6,1 reciprocal hexagonal lattice order (Figure 1e and h), indicating that this cationic stain revealed reproducible structural detail to a resolution of 2.2 nm. As documented in Figure 1f, over 80% of the correlation-averaged crystalline plaques revealed unit cells exhibiting a right-handed vorticity that was mainly due to the slightly skewed, low density stain-excluding connections between the inner and outer domains and the ''tilted'' orientation of the elliptical outer domains. In addition, the inner domains yielded a distinct triangular or pear-shaped morphology, instead of the more circular shape in the case of the SST-stained plaques (compare Figure 1f or i with Figure 1c). As illustrated in Figure 1i, less than 20% of the correlation-averaged crystalline plaques revealed unit cells exhibiting a left-handed vorticity (compare Figure 1f with Figure 1i), indicating that the corresponding AUM plaques (Figure 1g) had adsorbed to the EM grid by their opposite side, compared with those yielding a right-handed vorticity (Figure 1d, see below). In contrast to SST staining (see Figure 1c), UF staining also revealed faint stain-excluding bridges connecting the outer domains of neighboring AUM particles (see Figure 1f and i). These inter-particle connections were reproducible even without image enhancement. It is conceivable that these inherent structural features of the urothelial plaques represent physical connections between adjacent AUM particles. In a few single-patch averages, a faint stain-excluding domain could be depicted in the large, central cavity of the unit cell. However, this was not a reproducible structural feature of the 16 nm AUM particles, as it averaged out when correlation-averaged unit cells from different crystalline patches were combined.

Surface topography of AUM plaques

To visualize the surface topography of AUM plaques, we air-dried and then unidirectionally metal-shadowed bovine urothelial plaques (Figure 2a). As illustrated in Figure 2b, some of the observed membranes obviously belonged to vesicular structures. In these cases, it was clear that the cytoplasmic face of the plaque was quite smooth, whereas the luminal face exhibited a prominent surface texture consisting of hexagonally packed particles. These crystalline particle arrays revealed a lattice constant of 16.5 nm, and diffracted typically to the 2,1 reciprocal hexagonal lattice order, thus revealing reproducible structural detail to a resolution of 5.4 nm. Unlike the negatively stained unit cells, which were composed of two sets of six stain-excluding domains each (see Figure 1c, f and i), the unit cell of air-dried and metal-shadowed AUM plaques only exhibited six protrusions centered at a radius of about 4 nm, thus revealing a doughnut-like hexagonal unit cell morphology (data not shown). These results strongly suggested that the six protrusions depicted by metal shadowing were due predominantly to the six inner domains revealed in negatively stained AUM images (Figure 1c, f and i).

Since it is well known that, during air-drying, surface tension may cause irreversible distortion of the specimen's surface topography (Wildhaber *et al*., 1985), we also dehydrated AUM plaques by freeze-drying. As illustrated by the examples shown

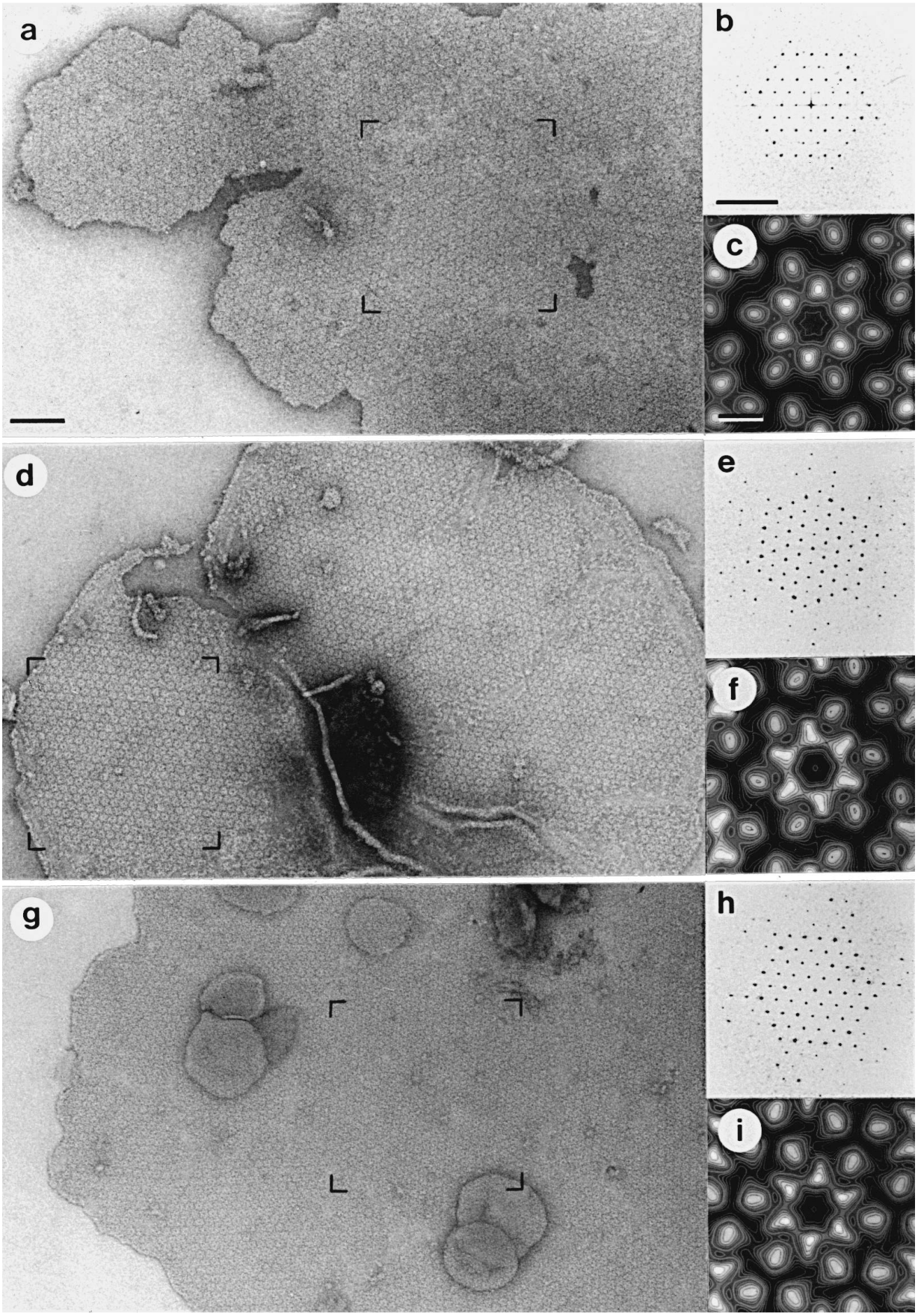

Figure 1.

in Figure 2b to d, the surface topography of the plaques, which had been adsorbed to the support film via their membranous, i.e. cytoplasmic, faces, appeared similar to that of the air-dried samples. It also revealed the strongly corrugated surface topography of the luminal 16 nm protein particles (Figure 2a), except that the resolution of structural detail was preserved to about 4.1 nm as indicated by the presence of the 2,2 reciprocal hexagonal lattice orders. Despite this improved resolution, the correlation-averaged and 6-fold symmetrical unit cell still revealed only six rather than 12 domains, representing predominantly the six inner domains seen in the negatively stained unit cells (compare with Figure 1c, f and i). However, unlike those of air-dried specimens, these radial domains were now clearly separated angularly, and had a short ''appendage'' attached to the left of their outer boundary, which probably represented the connecting bridge to the outer domain seen in negatively stained samples (compare Figure 2f with Figure 1c, f or i). These appendages gave rise to a tenuous but reproducible vorticity, and therefore established unequivocally the left-handed vorticity of the hexagonally packed 16 nm protein particles of the AUM plaques when viewed from their luminal side (i.e. when adsorbed with their cytoplasmic face to the support film; see also Figure 1i).

Three-dimensional reconstructions of AUM plaques

To examine the 3D architecture of the 16 nm AUM protein particles in more detail, we recorded tilt series of negatively stained AUM plaques, and computed their 3D mass density distribution, including data to a resolution of about 2.5 nm in the case of UF-stained specimens. Tilt series including 9 to 11 images ranging from –60° to +60° were recorded with doses of approximately 2000 e^-/nm^2 per tilted view (see Materials and Methods). Three representative sections (i.e. close to the lumen, in the middle of the particle, and close to the membrane) of SST-stained (Figure 3a to c) and UF-stained (Figure 3e to g and i to l) plaques are presented in Figure 3. For comparison with the corresponding 2D projection images (see Figure 1c, f and i), in Figure 3d, h and m, the corresponding sum images of all sections are displayed for each of the three averaged reconstructions. As observed previously by Brisson & Wade (1983) and Taylor & Robertson (1984), the vorticity of the structure changes when the 16 nm protein particle is cut at different *z*-levels (i.e. of different levels away from the membrane surface). While the AUM plaques that have been adsorbed onto the support film by their luminal faces show a right-handed vorticity in the sections near the tips through the 3D map (Figure 3a and e), the equivalent section through the 3D reconstruction of the AUM plaque that has been adsorbed to the grid via its membranous face shows the same vorticity as the correlation-average of the metal-shadowed specimen (compare Figure 3i with Figure 2f). The sections through the middle of the 3D reconstructions (Figure 3b, f and k) indicate only a minor handedness, while the sections through the AUM particle near the membranous side reveal again a distinct vorticity which is opposite to the one near the tips, i.e. left-handed for the AUM plaques that have been adsorbed *via* their luminal faces (Figure 3c and g), and right-handed for the AUM plaques that have been adsorbed *via* their cytoplasmic faces (Figure 3l).

A surface-rendered model of a 16 nm AUM particle computed from the 3D reconstruction of an SST-stained specimen (Figure 3a to c) which had been adsorbed onto the carbon support film *via* its luminal face (see Figure 1a) is shown in Figure 4a. In this case, the hexagon-shaped particle is composed of six V-shaped motifs, with the bottom of each V being anchored in the backing membrane, and the two tips of each V protruding into the lumen and representing one inner and one outer domain each. The mass density distribution within the 16 nm AUM particle of the UF-stained AUM plaques adsorbed with their luminal face to the support film (Figure 3e to g and Figure 4b) was similar, except that in this case the inner tip of one V was ''bridged'' to the outer tip of the next V. This distinct ''connectivity'' pattern of the V-shaped motifs gave rise to a 16 nm particle structure resembling a closed ''twisted ribbon'' embracing a central cavity (Figure 4b). A similar 3D structure was deduced from

Figure 1. Electron microscopy and image processing of negatively stained bovine asymmetric unit membrane (AUM) plaques. a, Sodium silicotungstate (SST)-stained AUM plaques. Note the stellate-shaped unit cells with a central stain-filled cavity. b, The diffraction pattern calculated from the area marked in a shows diffraction spots up to the 4,1 hexagonal lattice order indicating a resolution of 3.1 nm, while the radial correlation function (RCF) of independent correlation-averages yielded a resolution of 2.5 nm. c, Correlation-averaged and 6-fold symmetrized unit cell with the stain-excluding mass regions appearing bright, and the surrounding stain-filled areas appearing dark. This average reveals 12 stain excluding domains that are arranged on 2 concentric rings (r_{in} = 3.7 nm, r_{out} = 6.6 nm), each containing 6 identical domains. No significant connections between the inner and the outer domains or between neighboring unit cells are depicted. d and g, Uranyl formate-stained AUM membranes that have been adsorbed to the grid in opposite orientation. UF-stained plaques diffract significantly better than SST-stained plaques: the 6,1 hexagonal lattice order in e indicates a resolution of 2.2 nm (RCF: 1.5 nm), and the 5,3 reflection in h a resolution of 2.4 nm (RCF: 1.7 nm). The 6-fold symmetrized correlation averages (f and i) are mirror images of each other, as expected of a structure adsorbed to the support film in opposite orientation. The left-handed vorticity seen in the unit cell in i is found about five times less frequently than the right-handed vorticity seen in f. Scale bars represent 100 nm in a, $(4\ nm)^{-1}$ in b, and 5 nm in c.

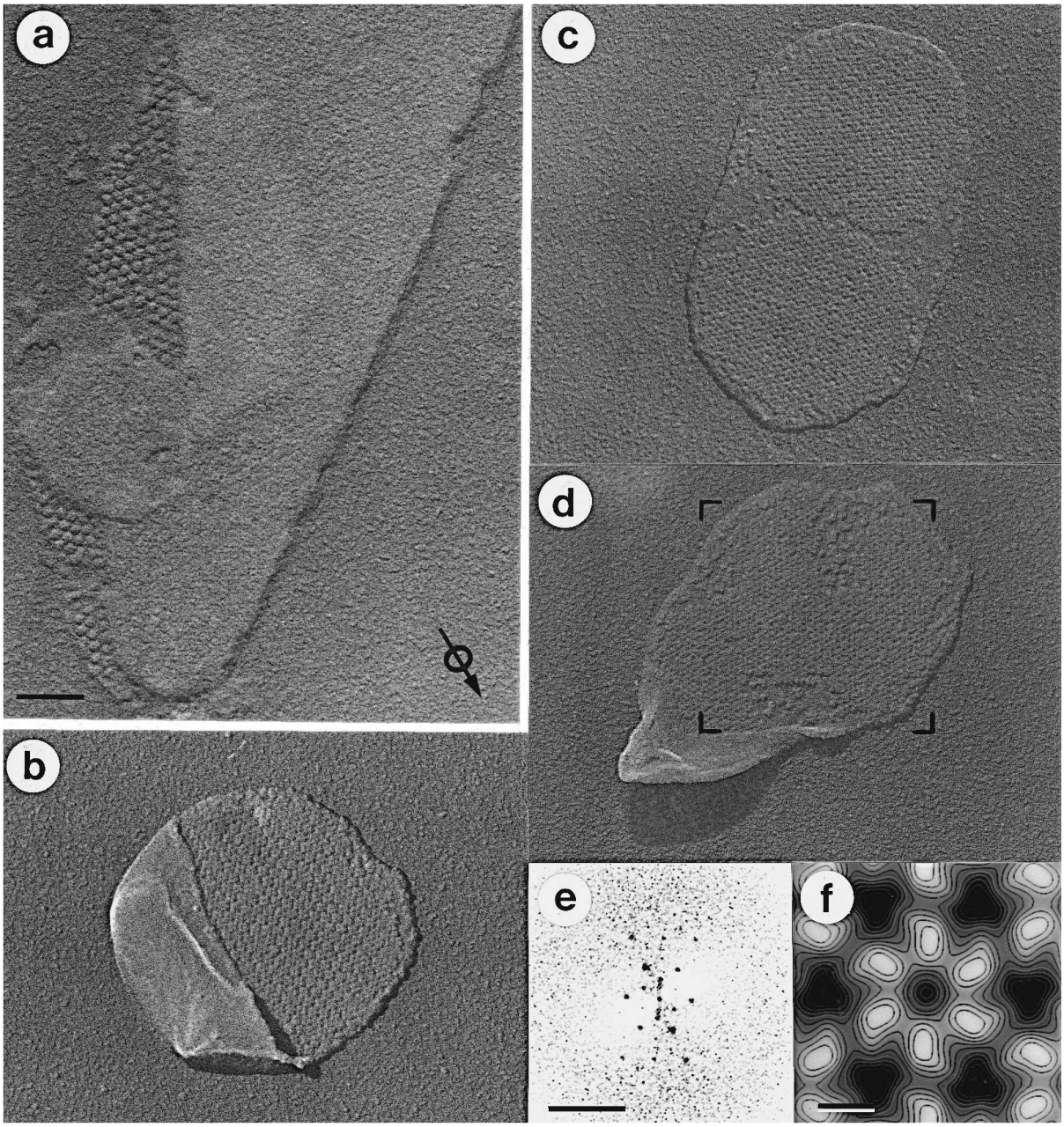

Figure 2. Electron microscopy and image processing of unidirectionally metal-shadowed bovine AUM plaques which have been either: a, air-dried or b to d, freeze-dried. a, An exceptionally large, partially folded AUM plaque, thus revealing both sides of the membrane. The cytoplasmic side exhibits a smooth texture with shallow hexagonal surface corrugations, whereas a small, folded over area of the corrugated luminal side reveals distinct, hexagonally packed particle arrays. b, A better structural preservation is achieved by quick-freezing and freeze-drying the sample before unidirectionally metal shadowing it. AUM vesicles reveal a smooth, featureless surface, but sometimes break open during adsorption to the support film, thereby exposing their luminal surface studded with hexagonally packed 16 nm particles. c, A fragment of the plasma membrane displays 2 AUM plaques that are separated by a structureless hinge area (see Introduction). d, The marked area was used to compute the diffraction pattern shown in e, which yields diffraction spots up to hexagonal lattice order 2,2, indicating a resolution of 4.1 nm (RCF: 3.1 nm). f, The resulting 6-fold symmetrized correlation-average reveals 6 distinct radially elongated protrusions showing a subtle left-handed vorticity. Scale bars represent 100 nm in a, $(4\ nm)^{-1}$ in e, and 5 nm in f. Arrow in a indicates the direction of metal shadowing.

UF-stained plaques that had been adsorbed to the grid *via* their cytoplasmic face (Figure 3i to l and Figure 4c). Comparing the features of the particles shown in Figure 4b and c, the bridged luminal tips of the former appear to be ''flattened'', probably as a result of the plaque–grid interactions. The inter-particle connections were best depicted in the sections near the membrane, as shown in Figure 3g and l. However, compared with the bulk of the AUM particles, the mass density of these inter-particle connections close to the membrane was relatively low, and thus did not show up at the contouring level

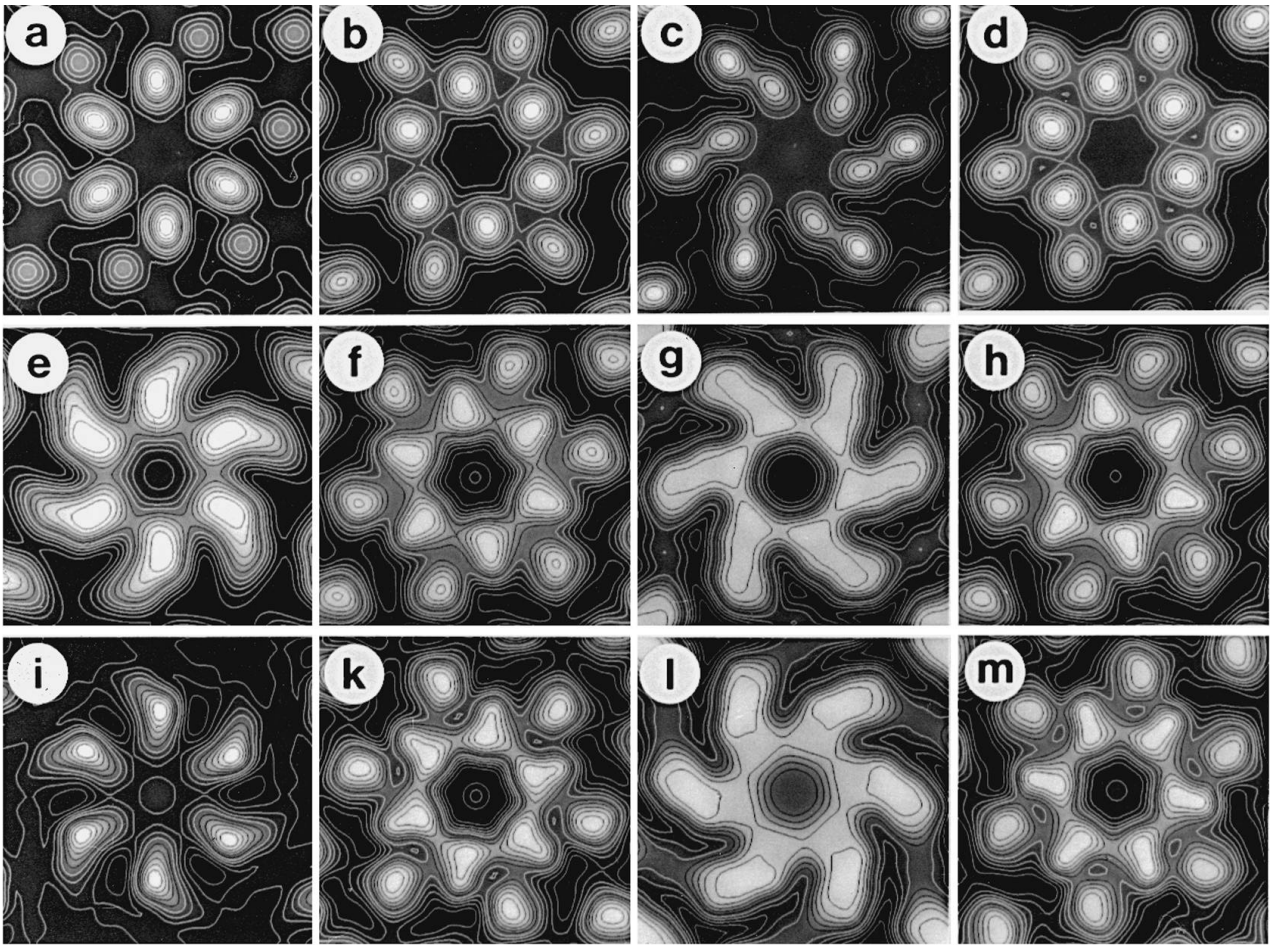

Figure 3. Sections through the 3D reconstructions of bovine AUM particles obtained from 3 differently stained plaques. a, b, c, d, SST-stained, with the luminal side of the plaque adsorbed to the carbon support film; e, f, g, h, UF-stained, same orientation as top row; i, k, j, m, UF-stained, with the cytoplasmic side of the plaque adsorbed. Each row displays 3 representative sections (a, e, and i, close to the lumen, b, f, and k, in the middle of the particle and c, g, l, close to the membrane), that are separated by 1.56 nm from the next section. In addition, the corresponding sum images of all sections of the 3 reconstructions are displayed in d, h and m.

chosen to produce the surface-rendered 3D models (see Figure 4b and c).

To improve the clarity of the basic architecture of the AUM particle, we computed vertical sections through the surface-rendered 3D density map of the UF-stained AUM particle shown in Figure 4c. The vertical sections in Figure 4f to i at the angular positions indicated in Figure 4e display in more detail the morphology of, and connections between, adjacent V-shaped subunits. Figure 4f illustrates that the luminal bridges are formed by the connections between an inner and an outer domain of two adjacent Vs, whereas Figure 4i illustrates how the bottom of each V-shaped subunit makes contact with the luminal surface of the backing membrane.

Overall, the luminal surface relief of the 16 nm AUM particles computed from freeze-dried and unidirectionally metal-shadowed plaques (Figure 2f) was in remarkably good agreement with the luminal sections of UF-stained AUM plaques (compare with Figure 3i). Like the surface-rendered representations of the 3D reconstructions from the UF-stained AUM plaques (compare Figure 4b and c), the surface relief (Figure 4d) exhibited a distinct left-handed vorticity when viewed from the luminal face.

STEM mass measurements

For mass measurements by scanning transmission electron microscopy (STEM), AUM plaques were adsorbed to 2 to 3 nm thick carbon films mounted on fenestrated plastic supports and either air-dried or freeze-dried in the pretreatment chamber of the STEM, so that they could be directly transferred into the high-vacuum chamber of the microscope (see Materials and Methods). Since, in most cases the ''empty'' membranes (i.e. those containing no regularly packed protein particles) could not be distinguished from the AUM plaques in low-dose STEM dark-field images (Figure 5a), air-dried specimens were metal-shadowed after STEM analysis (Figure 5b), and relocated in a conventional transmission EM (compare Figure 5a with Figure 5b). By this procedure, the AUM plaques containing hexagonally packed protein particles could be

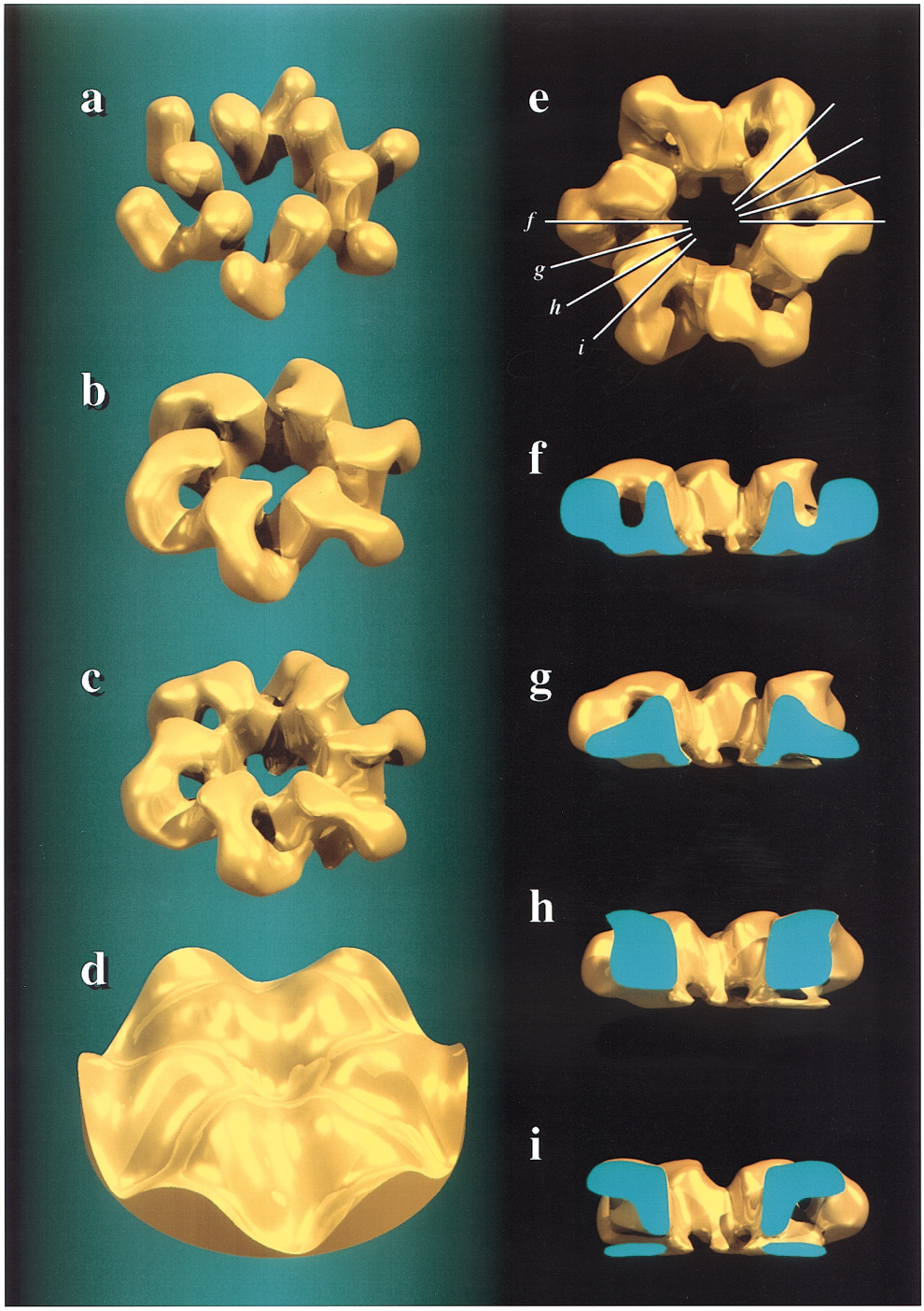

Figure 4. Surface-rendered 3-D reconstructions produced from negatively stained bovine AUM plaques, and surface relief computed from a quick-frozen / freeze-dried and unidirectionally metal shadowed bovine AUM plaque. a, The 3D map of the SST-stained AUM plaque that has been adsorbed with its luminal side facing the carbon support film reveals protein particles consisting of 6 V-shaped subunits arranged on a ring. b, The 3D map of a UF-stained AUM plaque adsorbed with the same orientation as the plaque in a. In this reconstruction, the inner tip of each V-shaped subunit is ''bridged'' to the outer tip of its adjacent V-shaped subunit; thus, the protein particle resembles a closed twisted ribbon embracing a central cavity. c, If the 3D map is reconstructed from an UF-stained plaque that has been adsorbed to the grid via its cytoplasmic face, the luminal surface is more textured, as it has not been compressed upon adsorption to the support film. d, The surface relief calculated from a quick-frozen / freeze-dried and unidirectionally metal-shadowed AUM plaque reveals mainly the inner domains and part of the luminal bridges to the outer domains. The outer domains and the connections between the inner and the outer domains close to the membrane are not resolved. All 4 structures are displayed at the same magnification and in the same orientation, i.e. viewed from the luminal side of the AUM plaques. e, The top view of the surface-rendered 3D mass map shown in c. The lines indicate the positions of the vertical cuts shown in f to i that are separated angularly by 15° each.

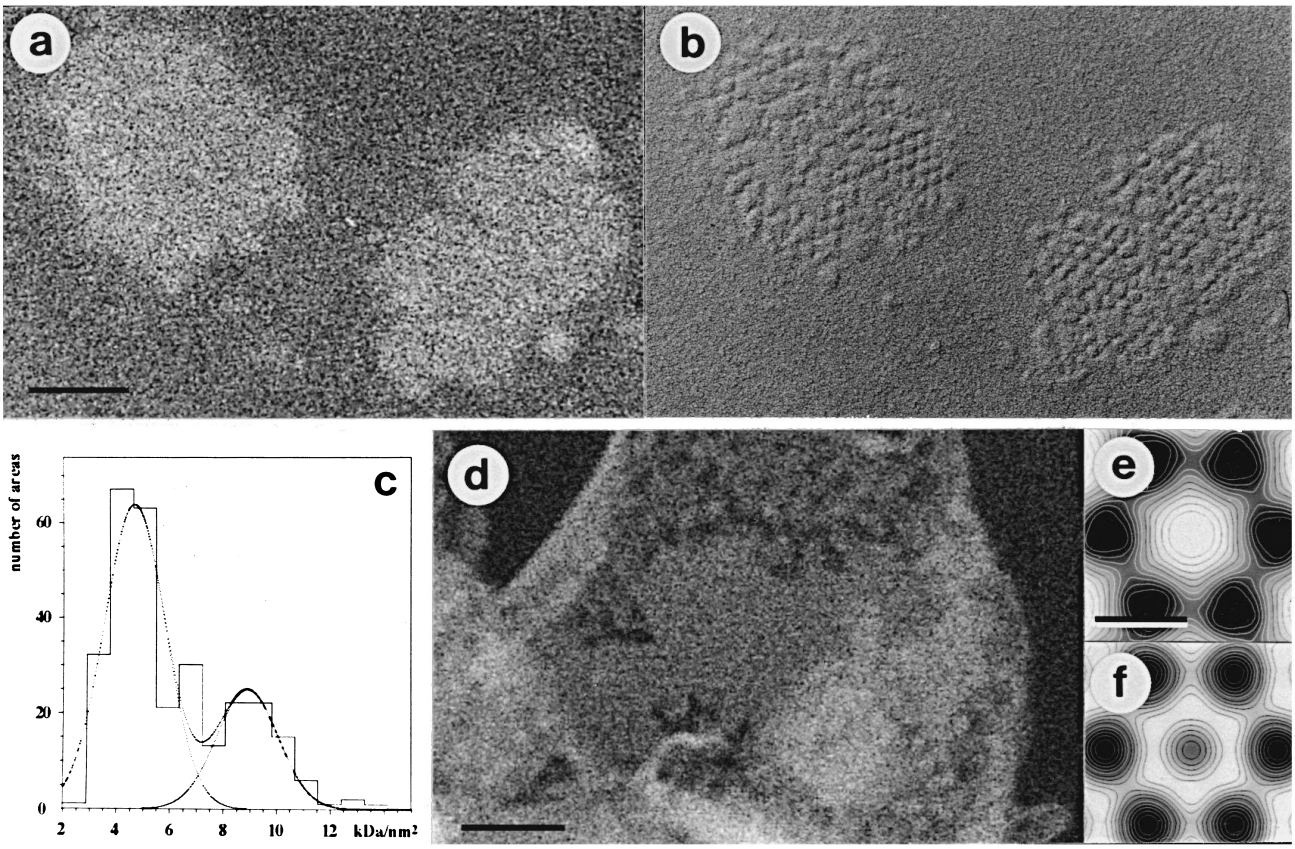

Figure 5. STEM mass analysis of freeze-dried / unstained bovine AUM plaques by scanning transmission electron microscopy (STEM). a, Low recording dose (100 e^- / nm^2) and contrast, elastic dark-field images of unstained AUM patches did not reveal the hexagonal packing of the luminal particles. b, However, the lattice became apparent, when after STEM analysis the unstained specimens were unidirectionally metal-shadowed and relocated in a TEM. c, The histogram displayed was obtained by evaluation of 296 MPA values. The first peak at 4.74 kDa / nm^2 represents the single-layered AUM structures, the second peak at 9.46 kDa / nm^2 results from double-layered AUM structures. d, In a few cases the hexagonal lattice of freeze-dried / unstained AUM plaques could already be depicted in STEM images. e, The crystalline area in d diffracted to the hexagonal lattice order 1,1, allowing the computation of the correlation averaged particle shown in e. Accordingly, the AUM particles reveal a distinct, stellate-shaped morphology exhibiting strong 6-fold symmetry; however, no fine structure was resolved. f, For comparison, a correlation-averaged particle of an AUM plaque negatively stained with UF was low-pass filtered to the same resolution as the average shown in e, i.e. including the hexagonal lattice order, 1,1. Scale bars represent 100 nm in a and d, and 10 nm in e.

identified. Accordingly, we pursued two types of analyses of the STEM data. First, we determined the mass per area (MPA) of a large number of membrane areas without preselection. Second, we only included those AUM plaques in the MPA histogram that revealed a hexagonal particle lattice by *a posteriori* unidirectional metal shadowing. As documented in Figure 5c, the MPA histograms of both types of mass analyses revealed two peaks, one at 4.47 kDa / nm^2 and a second one at 9.46 kDa / nm^2. These two peaks probably corresponded to the MPA of single- and double-layered AUM plaques, the latter probably representing collapsed vesicles (see Figure 2b). This indicates that most of the membranes chosen for mass analysis were actually not empty, but hexagonally packed with 16 nm AUM particles that were, however, not resolved in most of the low-dose STEM dark-field images.

As documented in Figure 5d, in a few cases, STEM dark-field images yielded membrane patches with an indication of a 16.5 nm hexagonal particle lattice that diffracted to the 1,1 reciprocal hexagonal lattice order. As indicated in Figure 5e, the averaged unit cells of such areas did not exhibit any vorticity, and the prominent cavity depicted in the center of negatively stained or metal-shadowed particles was absent. To find out whether this central cavity is simply not resolved in the freeze-dried, unstained samples imaged in the STEM, correlation-averages of UF-stained AUM plaques (e.g. Figure 1f or i) were low-pass-filtered to include the same diffraction orders (i.e. the 1,1 reciprocal hexagonal lattice order) as the STEM images. As documented in Figure 5f, in the negatively stained AUM plaques, the stain-filled central cavity is revealed even at this low resolution. Thus, it is conceivable that while there is indeed some mass present in the central cavity of the AUM particle, it becomes too disordered upon negative

staining and / or air drying, and is therefore averaged out upon correlation-averaging. Alternatively, the mass apparently being present in the central cavity of freeze-dried / unstained AUM plaques (Figure 5e) might represent an artifact due to collapse phenomena, since, for mass measurement, the structure was not stabilized by any stain or metal layer.

Discussion

Improved resolution of AUM plaques

An unexpected outcome of our analysis was the preservation of higher-resolution structural detail of the crystalline AUM plaques when negatively stained with UF instead of SST, i.e. an improvement from 3.1 nm to 2.2 nm. Another factor that may have contributed to the improved resolution revealed after negative staining with UF was the use of an improved, rapid isolation procedure for AUM plaques (Wu *et al*., 1994). Our data indicate that crystalline AUM plaques tend to disperse into smaller patches and eventually into single particles over time (data not shown). Anchorage of the AUM patches to an underlying cytoskeleton may prevent this from happening *in vivo* (Staehelin *et al*., 1972). Since the presumed AUM–cytoskeletal interaction is lost after isolation, rapidly isolated AUM plaques may retain a better crystalline structure, and hence yield 3D structural detail at a higher resolution.

AUM particles have a left-handed vorticity

Brisson & Wade (1983) found that the 6-fold symmetric 16 nm particles exhibited a distinct left-handed vorticity in about 80% of their plaque images, suggesting a preferential adsorption of the plaques to the support film. However, since negative staining provides a through-projection image of the structure, *a priori* this observation cannot determine which face of an AUM plaque has adsorbed to the support film. We have solved this ambiguity by visualizing the surface topography of adsorbed AUM plaques. The observation that most AUM plaques appeared ''smooth'' after unidirectional metal-shadowing indicated that they had adsorbed preferentially with their textured, luminal side facing the support film. Moreover, correlation averages calculated from the few plaques that had adsorbed to the support film by their cytoplasmic side yielded a left-handed vorticity of their hexagonal 16 nm particles after freeze-drying / unidirectional metal shadowing (see Figure 2f), thus confirming the left-handedness of the AUM particles when viewed from their luminal side.

Our observation of a smooth cytoplasmic face of the AUM plaques after metal shadowing agrees with previous EM data. Wade & Brisson (1984) observed a fine periodic lattice structure, which they believed was due to the sagging of the air-dried membrane between the supporting protein particles whose luminal face was in contact with the flat carbon support film. The smoothness of the cytoplasmic face of AUM plaques prompted some earlier investigators to speculate that the protein subunits of the AUM plaques may not penetrate the lipid bilayer. We now know from the deduced primary sequences of the uroplakins, however, that all four major uroplakins possess stretches of hydrophobic amino acid residues that are long enough to form transmembrane α-helices (Yu *et al*., 1994). Moreover, it is interesting to note that three of the four major uroplakins, UPIa, UPIb and UPIII, have very small cytoplasmic domains. UPIII is the only AUM subunit that has a significant cytoplasmic domain, which may interact with some component(s) of the underlying cytoskeleton. This 50 residue cytoplasmic domain of UPIII harbors multiple potential phosphorylation sites that may be involved in regulating AUM–cytoskeleton interaction (Wu & Sun, 1993). The smoothness of the cytoplasmic face of crystalline AUM plaques indicates that the cytoplasmic domain of UPIII may be too small and / or become too disordered to be visualized under our preparation and imaging conditions, once the plaques have been dissociated from the underlying cytoskeleton. EM localization of epitopes on this 50 residue cytoplasmic domain of UPIII on the cytoplasmic side of the isolated AUM plaques will be needed to test this theory (see below).

The 16 nm AUM particle reveals a closed ''twisted ribbon'' structure

Our 3D reconstructions of UF-stained AUM plaques revealed that each 16 nm particle has six distinct ''feet'' that are in contact with the luminal surface of the lipid bilayer (see Figure 3c, g and l, and Figure 4i). This spatially confined anchorage of the AUM particles causes severe constraints as to where within the hexagonal unit cell the uroplakin molecules traverse the lipid bilayer. Moreover, it may explain why trypsinization can easily detach the 16 nm particles from the membrane (Caruthers & Bonneville, 1980).

The 3D maps of UF-stained AUM plaques exhibited a slightly different surface topology, depending on whether the plaques had been adsorbed to the carbon support film by their luminal or cytoplasmic face. Plaques with their smooth, cytoplasmic face adsorbed to the support film revealed 16 nm particles with distinctly textured luminal bridges joining adjacent inner and outer domains (Figure 4c), whereas plaques with their textured luminal face in contact with the support film revealed 16 nm particles with their luminal bridges squashed flat (Figure 4b). This squashing is most likely caused by the strong interactive forces exerted between the protein moiety and the support film. This squashing did not significantly affect the measured thickness of the 16 nm particles, however, which in both cases was approximately 5 nm. This is probably due to the fact that squashing of the 16 nm particles, when adsorbed to the support film by their luminal face, is matched by incomplete stain

embedding of AUM plaques adsorbed to the support film via their cytoplasmic face.

The luminal surface relief reconstructed from freeze-dried / unidirectionally metal-shadowed plaques (Figure 4d) was in remarkable agreement with the 3D reconstruction computed from UF-stained plaques that had been adsorbed to the support film by their cytoplasmic face (Figure 4c). However, the surface relief predominantly revealed the six inner domains, with indications of the bridges to the outer domains. The outer domains—best resolved in the SST-stained 3D reconstruction (Figure 4a)—are largely invisible in this preparation, probably because the surface elevation of the six outer domains was too low to be accessible to metal evaporation at the elevation angles ($\leqslant 40°$) used for shadowing.

Structural implications

On the basis of a 236 nm^2 unit cell area (Figure 5e) and the 4.74 kDa / nm^2 mass per area (MPA) determined by quantitative STEM (Figure 5c), we calculated a MPU of 1120 kDa for bovine urothelial plaques. This MPU value represents the total mass of the extramembranous and transmembranous protein parts, the sugar moieties, and the lipid bilayer.

Secondary structure prediction revealed one transmembrane helix each for uroplakins II and III, and four transmembrane helices each for uroplakins Ia and Ib (Wu & Sun, 1993; Lin *et al*., 1994; Yu *et al*., 1994). If we assume that there is one copy each of the four major uroplakins per asymmetric unit [i.e. 27 kDa (UPIa) + 28 kDa (UPIb) + 15 kDa (UPII) + 47 kDa (UPIII) = 117 kDa] this yields a total mass of 702 kDa for the protein plus sugar moieties of the 16 nm AUM particle. If we subtract the mass of the 60 transmembrane helices per unit cell, i.e. taking an average of 25 residues per transmembrane helix and an average mass of 105 Da per amino acid, we are left with *544 kDa* for the extramembranous mass of the 16 nm particle. As an α-helix has a cross-section of $\sim 1\ nm^2$, the 60 transmembrane helices account for $\sim 60\ nm^2$ of the 236 nm^2 unit cell area, thus leaving 176 nm^2, or a mass of 475 kDa (i.e. with a MPA of 2.7 kDa / nm^2 for a typical lipid bilayer; Walz *et al*., 1994*a*) for the lipid moiety per unit cell. If we now subtract this lipid contribution from the total 1120 kDa unit cell mass, we obtain 645 kDa for its protein plus sugar moiety or, upon further subtraction of the 60 transmembrane helices, *487 kDa* for the extramembranous MPU. This latter, measured mass comes very close to the 544 kDa mass calculated from the 16 nm particle's assumed subunit stoichiometry and transmembrane helices (see above). For comparison, from the 3D reconstructions of UF-stained AUM plaques (see Figure 4b and c) we calculated an extramembranous MPU of roughly 450 kDa. It should be stressed, however, that this latter MPU strongly depends on the contouring level chosen, and thus could become as little as 300 kDa or as great as 600 kDa. Nevertheless, it is remarkable that both the calculated and measured MPUs lie well within these estimated limits.

In spite of this good agreement, there are obviously several other possible stoichiometries that *a priori*, cannot be ruled out (see below). Nevertheless, we can estimate a minimum and maximum amount of protein that can be included in the AUM structure. On the one hand, if we assume the uroplakins to possess no transmembrane domains, the total protein plus sugar moiety would account for a MPU of about 480 kDa (i.e. 1120 kDa, minus 640 kDa, the latter being the mass of a 236 nm^2 lipid bilayer). On the other hand, it is very unlikely that less than 50% of the unit cell area is padded with lipid, thus yielding a lipid MPU of less than 320 kDa. The same calculation as above (i.e. 1120 kDa minus 320 kDa) allows for a MPU of 800 kDa for the protein plus sugar moiety of the entire unit cell. A mass of 645 kDa per asymmetric unit for the protein plus sugar moiety, as determined from the assumptions made above, lies well within these estimated extremes.

The four major uroplakins can be divided into two groups based on their deduced amino acid sequences. UPIa and UPIb both contain four hydrophobic transmembrane segments, are 39% identical, and are members of a recently identified superfamily of transmembrane proteins (Yu *et al*., 1994). In contrast, UPII and UPIII yield novel amino acid sequences, and show no homology to any other known proteins. Interestingly, these two uroplakins share a stretch of about ten amino acid residues, located at the extracellular N-terminal end of their potential single transmembrane segment (Lin *et al*., 1994; Wu & Sun, 1993), suggesting that UPII and UPIII are somewhat structurally related, thus forming a uroplakin group that is distinct from the UPIa / UPIb group. As yet, the structural significance of these two distinct uroplakin groups is unclear.

For the ultimate elucidation of the uroplakin stoichiometry within the AUM unit cell, we have generated a panel of rabbit antisera against 15 synthetic peptides representing different segments of the extracellular domains of the four uroplakins (X.-R. Wu, unpublished results). EM localization of these epitopes on different domains of isolated AUM plaques should allow us to eventually determine the subunit composition of the 16 nm AUM particles, and to define the contributions of individual uroplakins to the distinct morphological domains of the AUM particles.

Functional implications

Although AUM plaques are perhaps the most prominent structures in terminally differentiated urothelial cells, and the genes encoding their protein constituents, the uroplakins, are known to be expressed in a bladder-specific and differentiation-dependent fashion, the functional significance of this remarkable biomembrane remains unclear. Possible functions of AUM include serving as a permeability barrier, as a means of stabilizing the apical bladder

surface, and as a supramolecular device to change the surface area of the plasma membrane. Hicks (1965) was amongst the earliest to suggest that AUM may serve as a permeability barrier. This notion was dismissed by many investigators, based on the fact that the AUM plaques cover only $\leqslant$80% of the apical surface, and therefore cannot be the sole mechanism to achieve this function. Our 3D reconstructions of AUM plaques have confirmed earlier data (Brisson & Wade, 1983; Wade & Brisson, 1984) that suggest that the central cavity of the 16 nm protein particle does not penetrate the lipid bilayer. Thus, despite the gross resemblance of the AUM particle to the gap junction channel (which is 12 nm in diameter, has only six structural domains, and forms less-ordered crystalline arrays *in situ*), the AUM particles are highly unlikely to serve as ion channels. That structures containing uroplakin may serve as an effective permeability barrier within the urothelium was shown recently by Chang *et al*. (1995) who demonstrated that vesicles of rabbit urothelium which contain uroplakin, formed by the luminal surface membrane, are unusually impermeable to urea, water and ions.

In summary, we have proposed a closed twisted-ribbon model to account for the 3D structure of the 16 nm protein particles that naturally form 2D crystals in bovine urothelium. Since the ultra-structural organization and uroplakin composition of these particles are highly conserved during mammalian evolution, the 3D architecture that we propose here for bovine AUM is probably applicable to the AUM of other mammalian species, including man and mouse (Wu *et al*., 1994). Although some of the structural features described in our model are, in retrospect, present in some of the data presented earlier (Brisson & Wade, 1983; Wade & Brisson, 1984), the higher resolution that we have achieved through an improved isolation procedure of AUM plaques and the use of UF as a negative stain makes these structural features stand out more clearly. These include the extracellular protein topology of the 16 nm particle, which is best described as a closed twisted ribbon embracing a central cavity, and the distinct inter-particle connections that may contribute to the unusual degree of insolubility of the AUM plaques in a number of non-ionic detergents. Finally, we have determined for the first time the MPU of AUM, thus providing structural constraints on how uroplakins and other membrane constituents interact to form this remarkable biomembrane.

Materials and Methods

Membrane preparation and electron microscopy

Asymmetric unit membranes were isolated from bovine urinary bladders using a sucrose density gradient procedure (Wu *et al*., 1990, 1994). The purified AUM plaques were adsorbed to glow-discharged grids, washed in double-distilled water, and negatively stained with either 0.75% (w/v) UF (pH 4.2) or 2 (w/v) SST (pH 7.0). To obtain information on their surface topography, adsorbed AUM plaques were washed in double-distilled water, and quick frozen by plunging them into a mixture of liquid propane and isopentane. After freeze-drying in a Balzers BAF 300 freeze-fracture unit at –80°C for five hours, the membranes were unidirectionally shadowed at the same temperature with platinum–iridium at an elevation angle of 40°. Images were recorded on Kodak SO-163 film at a nominal magnification of ×50,000 under low-dose conditions using a Hitachi H-7000 or H-8000 transmission electron microscope operated at 100 kV. The magnification was calibrated using negatively stained catalase crystals (Wrigley, 1968).

Image processing

For the assessment of the crystallinity of the AUM plaques and the microscope settings, micrographs were screened with an optical diffractometer (Aebi *et al*., 1973). Suitable micrograph areas were digitized and transferred to a VAX station 3100 using an Eikonix 850 CCD imaging camera equipped with a Zeiss S planar objective lens. First, a blank frame was recorded and stored for on-line subtraction of background noise due to gain and bias variations of the 4096-pixel linear CCD array. In addition, 3×3 pixel areas were averaged and stored as single pixels corresponding to a spatial separation of $\sim$0.64 nm in the specimen plane. Two methods were employed for calculating averages using the SEMPER image processing system (Saxton *et al*., 1979): (1) quasi-optical Fourier peak filtration was used for the evaluation of the crystal quality and unit cell morphology (Aebi *et al*., 1973) and (2) correlation averaging was used to eliminate intrinsic lattice disorder by locating the unit cells precisely using one AUM unit cell as the reference (Saxton & Baumeister, 1982). The correlation-averaged unit cell was finally 6-fold symmetrized. Surface reliefs of unidirectionally metal-shadowed specimens were computed using the method of Smith & Kistler (1977). For 3D reconstructions, tilt series were recorded at minimum dose with tilt angles ranging from 0°, $\pm$25°, $\pm$45°, $\pm$50°, $\pm$55° to $\pm$60° (Walz *et al*., 1994*b*). Crystalline AUM patches were individually processed, and stacks of horizontal sections with a thickness of 0.25 nm were computed using the SEMPER image processing package (Saxton *et al*., 1979). The 3D reconstruction stacks were visualized by surface rendering using MapView, a marching cube algorithm (Lorensen & Cline, 1987) implemented in our laboratory on a Silicon Graphics Iris Crimson computer.

STEM mass measurements

AUM plaques were adsorbed to glow-discharged grids that were covered with a thin carbon film which was mounted on a fenestrated plastic film enhanced with a thick carbon film, and washed extensively in double-distilled water. The samples were then plunged into liquid nitrogen, and freeze-dried inside the specimen chamber of a scanning transmission electron microscope (STEM) at –80°C (Engel & Meyer, 1980). Elastic annular dark-field images 512×512 pixels in size were acquired digitally using a Vacuum Generators (East Grinstead, England) STEM HB-5 operated at 80 kV, with either a pixel size of 1.87 nm (i.e. ×100,000 nominal magnification) or 0.93 nm (i.e. ×200,000 nominal magnification) and at doses between 100 and 800 e^-/nm^2 (Engel, 1978). Processing of the digital STEM images for mass determination was carried out as described by Müller *et al*. (1992). Mass data were compiled in histograms, which were fitted by Gaussian profiles using a Marquardt algorithm (Bevington, 1969).

Acknowledgements

We thank Hedi Frefel, Margrit Steiner and Marlies Zoller for expert photographic work. This work was supported by research grants from the Swiss National Science Foundation (31-39691.93 to U.A., and 31-32536.91 to A.E.), by grants from the National Institutes of Health (DK39753, DK47529 and DK49469 to T.-T.S.), a predoctoral fellowship from the Roche Research Foundation (to T.W.), the Department of Education of the Kanton Basel-Stadt, and the M.E. Müller Foundation of Switzerland.

References

Aebi, U., Smith, P. R., Dubochet, J., Henry, C. & Kellenberger, E. (1973). A study of the structure of the T-layer of Bacillus brevis. *J. Supramol. Struct.* **1**, 498–522.

Bevington, P. (1969). *Data Reduction and Error Analysis for the Physical Sciences*, pp. 235–242. McGraw-Hill Book Comp., New York.

Brisson, A. & Wade, R. H. (1983). Three-dimensional structure of luminal plasma membrane protein from urinary bladder. *J. Mol. Biol.* **166**, 21–36.

Caruthers, J. M. S. & Bonneville, M. A. (1980). The asymmetric unit membrane (AUM) structure in the lumenal plasma membrane of urothelium: The effect of trypsin on the integrity of the plaques. *J. Ultrastruct. Res.* **71**, 288–302.

Chang, A., Hammond, T. G., Sun, T.-T. & Zeidel, M. L. (1995). Permeability properties of the mammalian bladder apical membrane. *Am. J. Physiol*. **267**, 1483–1492.

Cowan, S. W., Schirmer, T., Rummel, G., Steiert, M., Ghosh, R., Pauptit, R. A., Jansonius, J. N. & Rosenbusch, J. P. (1992). Crystal structures explain functional properties of two E. coli porins. *Nature (London)*, **358**, 727–733.

Deisenhofer, J., Epp, O., Miki, K., Huber, R. & Michel, H. (1984). X-ray structure analysis of a membrane protein complex. Electron density map at 3 Å resolution and a model of the chromophores of the photosynthetic reaction centre from *Rhodopseudomonas viridis*. *J. Mol. Biol.* **180**, 385–398.

Deisenhofer, J., Epp, O., Miki, K., Huber, R. & Michel, H. (1985). Structure of the protein subunits in the photosynthetic reaction centre of Rhodopseudomonas viridis at 3 Å resolution. *Nature (London)* **318**, 618–624.

Engel, A. (1978). Molecular weight determination by scanning transmission electron microscopy. *Ultramicroscopy*, **3**, 273–281.

Engel, A. & Meyer, J. (1980). Preparation of unstained protein structures for mass determination by electron scattering. *J. Ultrastruct. Res.* **72**, 212–222.

Engel, A., Hoenger, A., Hefti, A., Henn, C., Ford, R. C., Kistler, J. & Zulauf, M. (1992). Assembly of 2-D membrane protein crystals: Dynamics, crystal order, and fidelity of structure analysis by electron microscopy. *J. Struct. Biol.* **109**, 219–234.

Henderson, R., Baldwin, J. M., Ceska, T. A., Zemlin, F., Beckmann, E. & Downing, K. H. (1990). Model for the structure of bacteriorhodopsin based on high-resolution electron cryo-microscopy. *J. Mol. Biol.* **213**, 899–929.

Hicks, R. M. (1965). The fine structure of the transitional epithelium of rat ureter. *J. Cell Biol.* **26**, 25–48.

Hicks, R. M. & Ketterer, B. (1969). Hexagonal lattice of subunits in the thick luminal membrane of the rat urinary bladder. *Nature (London)*, **224**, 1304–1305.

Jap, B. K., Zulauf, M., Scheybani, T., Hefti, A., Baumeister, W., Aebi, U. & Engel, A. (1992). 2D crystallization: from art to science. *Ultramicroscopy*, **46**, 45–84.

Knutton, S. & Robertson, J. D. (1976). Regular structures in membranes: The lumenal plasma membrane of the cow urinary bladder. *J. Cell Sci.* **22**, 355–370.

Kühlbrandt, W. (1992). Two-dimensional crystallization of membrane proteins. *Q. Rev. Biophys.* **25**, 1–49.

Kühlbrandt, W., Wang, D. N. & Fujiyoshi, Y. (1994). Atomic model of plant light-harvesting complex by electron crystallography. *Nature (London)*, **367**, 614–621.

Lin, J. H., Wu, X. R., Kreibich, G. & Sun, T.-T. (1994). Precursor sequence, processing, and urothelium-specific expression of a major 15 kDa protein subunit of asymmetric unit membrane. *J. Biol. Chem.* **269**, 1775–1784.

Lorensen, W. & Cline, H. E. (1987). Marching cubes: a high resolution 3D surface construction algorithm. *Computer Graphics*, **21**, 163–169.

Müller, S., Goldie, K. N., Bürki, R., Häring, R., Engel, A. & Reichelt, R. (1992). Factors influencing the precision of quantitative scanning transmission electron microscopy. *Ultramicroscopy*, **46**, 317–334.

Porter, K. R. & Bonneville, M. A. (1963). *Fine Structure of Cells and Tissues* 4th edit., Lea & Febiger, New York.

Robertson, J. D. & Vergara, J. (1980). Analysis of the structure of intramembrane particles of the mammalian urinary bladder. *J. Cell. Biol.* **86**, 514–528.

Saxton, W. O. & Baumeister, W. (1982). The correlation averaging of a regularly arranged bacterial cell envelope protein. *J. Microsc.* **127**, 127–138.

Saxton, W. O., Pitt, T. J. & Horner, M. (1979). Digital image processing: the SEMPER system. *Ultramicroscopy*, **4**, 343–354.

Smith, P. R. & Kistler, J. (1977). Surface reliefs computed from micrographs of heavy metal-shadowed specimens. *J. Ultrastruct. Res.* **61**, 124–133.

Staehelin, L. A., Chlapowski, F. J. & Bonneville, M. A. (1972). Lumenal plasma membrane of the urinary bladder. I. Three-dimensional reconstruction from freeze-etch images. *J. Cell Biol.* **52**, 73–91.

Taylor, K. A. & Robertson, J. D. (1984). Analysis of the three-dimensional structure of the urinary bladder epithelial cell membranes. *J. Ultrastruct. Res.* **87**, 23–30.

Vergara, J., Longley, W. & Robertson, J. D. (1969). A hexagonal arrangement of subunits in membrane of mouse urinary bladder. *J. Mol. Biol.* **46**, 593–596.

Wade, R. H. & Brisson, A. (1984). Three-dimensional structure of bladder membrane protein. *Ultramicroscopy*, **13**, 47–56.

Walz, T., Smith, B. L., Zeidel, M. L., Engel, A. & Agre, P. (1994*a*). Biologically active 2-dimensional crystals of aquaporin CHIP. *J. Biol. Chem.* **269**, 1583–1586.

Walz, T., Smith, B. L., Engel, A. & Angre, P. (1994*b*). The three-dimensional structure of human erythrocyte aquaporin CHIP. *EMBO J.* **13**, 2985–2993.

Weiss, M. S., Kreusch, A., Schiltz, E., Nestel, U., Welte, W., Weckesser, J. & Schulz, G. E. (1991). The structure of porin from Rhodobacter capsulatus at 1.8 Å resolution. *FEBS Letters*, **280**, 379–382.

Wildhaber, I., Gross, H., Engel, A. & Baumeister, W. (1985). The effects of air-drying and freeze-drying on the structure of a regular protein layer. *Ultramicroscopy*, **16**, 411–422.

Wrigley, N. G. (1968). The lattice spacing of crystalline catalase as an internal standard of length in electron microscopy. *J. Ultrastruct. Res.* **24**, 454–464.

Wu, X.-R. & Sun, T.-T. (1993). Molecular cloning of a 47 kDa tissue-specific and differentiation-dependent

urothelial cell surface glycoprotein. *J. Cell Sci.* **106**, 31–43.

Wu, X.-R., Manabe, M., Yu, J. & Sun, T.-T. (1990). Large scale purification and immunolocalization of bovine uroplakins I, II, and III. *J. Biol. Chem.* **265**, 19170–19179.

Wu, X.-R., Lin, J.-H., Walz, T., Häner, M., Yu, J., Aebi, U. & Sun, T.-T. (1994). Mammalian uroplakins: A group of highly conserved urothelial differentiation-related membrane proteins. *J. Biol. Chem.* **269**, 13716–13724.

Yu, J., Manabe, M., Wu. X.-R., Xu, C., Surya, B. & Sun, T.-T. (1990). Uroplakin I: A 27-kD protein associated with the asymmetric unit membrane of mammalian urothelium. *J. Cell Biol.* **111**, 1207–1216.

Yu, J., Lin, J. H., Wu. X. R. & Sun, T.-T. (1994). Uroplakin-Ia and uroplakin-Ib, two major differentiation products of bladder epithelium, belong to a family of four transmembrane domain (4TM) proteins. *J. Cell Biol.* **125**, 171–182.

Edited by R. Huber

(Received 7 November 1994; accepted 20 February 1995)